In Proceedings of "High Level Radioactive Waste Management Conference"
April, 1993 Las Vegas, NV USA

FULL-FIELD DYE CONCENTRATION MEASUREMENT WITHIN SATURATED/UNSATURATED THIN SLABS OF POROUS MEDIA

Dennis L. Norton
U. of Arizona, Department of Hydrology,
Tucson, AZ., 85721
(505-844-0945)

Robert J. Glass
Sandia National Laboratory, Geoscience Center,
Division 6115, Albuquerque, NM., 87185
(505-844-0945)

ABSTRACT

This paper presents a full-field dye concentration measurement technique that extends our experimental capabilities to the measurement of transient dye concentration fields within steady state flow fields under unsaturated or saturated conditions. Simple light absorption theory provides a basis for translating images into high resolution dye concentration fields. A series of dye pulse experiments that demonstrate the combined use of the full-field saturation and dye concentration techniques was conducted at four different degrees of saturation. Each of these experimental sequences was evaluated with respect to mass balance, the results being within 5% of the known dye mass input. An image windowing technique allowed us to see increased dispersion due to decreasing moisture content, tailing of concentration at the rear of the dye pulse and slight velocity changes of the dispersive front due to changes in moisture content.

The exceptional resolution of dye concentration in space and time provided by this laboratory technique allows systematic experimentation for examining basic processes affecting solute transport within saturated/unsaturated porous media. Future challenges for this work will be to use these techniques to analyze more complex systems involving heterogeneities, scaling laws, and detailed investigations of the relationship between transverse and longitudinal dispersion in unsaturated media.

INTRODUCTION

Over the past ten years increasing attention has been focused on investigating the relationships among spatial variability of hydraulic conductivity, solute dispersion, and characteristic length scales within the system of interest. The goal has been to improve predictions of field-scale transport of solutes through geologic material. Theoretical approaches that employ the statistical properties of the hydraulic conductivity field to predict solute dispersion have been developed by a number of researchers [1,2,3,4]. Stochastic numerical simulation has been used extensively to investigate transport in both saturated [5,6,7,8] and unsaturated systems [9,10]. While these theoretical and numerical investigations of dispersion in porous media are widespread, field studies and controlled laboratory experiments are sparse. There is a need for experimental techniques that allow us to systematically test and challenge theory for these complex systems [11,12].

Glass [13] designed a two-dimensional experimental system to challenge current understanding of flow and transport under both unsaturated and saturated heterogeneous porous media. The system is composed of a thin (10-100 grain diameters) but extensive (30-60 cm) slab chamber that is filled with translucent silica sands. Permeability and capillary properties of the media are controlled by varying the grain size distribution and bulk density of the sand pack. Heterogeneity structure is controlled through a variety of filling and packing techniques that allow systematic variation of the scale and intensity of the heterogeneity. These techniques produce homogeneous packs or highly heterogeneous packs containing layering and crossbedding. During unsaturated flow experiments, moisture content fields are measured in real time with exceptional accuracy and spatial resolution using a full-field, transmitted light digital imaging technique [14,15].

In this paper we introduce a full-field dye concentration measurement technique that extends our experimental capabilities to the measurement of transient dye concentration fields within steady state flow fields under both unsaturated and saturated conditions. First we present the simple absorption theory on which the technique is based. We then describe the experimental system and present a series of experiments that demonstrate the combined use of the full-field saturation and dye concentration techniques. Finally, we conclude with a discussion of our results.

THEORETICAL DEVELOPMENT

In an unsaturated, translucent porous media (sand), the indices of refraction are more closely matched at the water-sand interface than at the air-sand interface. As a result, there is a greater transmission of visible light where saturation is higher.

Recognizing that this effect far outweighs the differential light absorption of the air and the water, Hoa [16] developed a functional relation describing this behavior as

$$I_{out} = \{I_{dry}\}\left\{\tau_{sw}/\tau_{sa}\right\}^{2p} \qquad (1)$$

where p is the number of pores filled with de-ionized water (DI) at some moisture content; τ_{sa} and τ_{sw} are the light transmission factors for the sand-air and sand-water interfaces respectively (τ_{sa}=0.946, τ_{sw}=0.991); I_{out} is the emergent light intensity and I_{dry} represents the light transmittance through the dry sand pack. Equation (1) assumes that the light transmittance factors are not functions of wavelength. Making use of this principle, Glass et. al. [14] backlit a thin slab of translucent silica sand and captured high resolution digital images of two-dimensional transient moisture content fields. Using the approximation that $Sk=p$ where S is the saturation and k is the average number of pores through which the light passes, Tidwell and Glass [15] developed a normalization and calibration procedure for the light technique (equation 2) which, when compared to x-ray and gamma ray attenuation methods, showed exceptional accuracy for saturation. Saturation is given by:

$$S = \frac{\ln\left[I_n\left[\left(\tau_{sw}/\tau_{sa}\right)^{2k} - 1\right] + 1\right]}{2k\ln\left[\tau_{sw}/\tau_{sa}\right]} \qquad (2)$$

where I_n is the normalization of the image of interest (I) on a pixel by pixel basis between the bright saturated image (I_{sat}) and the dark dry image (I_{dry}).

Extension of this light transmission and digital imaging method to visualize dye concentration fields within the unsaturated slab of porous material is expected to be straightforward for dyes that either absorb or emit light (fluoresce). Here we explore light absorbing dyes and make use of the exponential Beer-Lambert law for monochromatic light absorption by the dye. Equation (1) can be modified by assuming that the exponential Beer's law attenuates in a multiplicative way:

$$I_{out} = \{I_{dry}\}\left\{\tau_{sw}/\tau_{sa}\right\}^{2Sk}\{exp-(C\mu L_d)\} \qquad (3)$$

where C is dye concentration, μ light absorption coefficient and L_d is distance traveled through the dyed water. In writing equation (3) we have assumed that the indices of refraction are not functions of the dye concentration. Solving equation (3) for C and forming the C/C_o ratio yields the working relationship for concentration

$$C/C_o = \frac{\ln[I_d] - \ln[I_{nd}]}{\ln[I_{dss}] - \ln[I_{nd}]} \qquad (4)$$

Where (I_{nd}) is a steady-state initial moisture content image with no dye that is captured immediately prior to the release of a dye pulse. As the dye pulse front moves through the chamber a series of images (I_d) are taken . Once the concentration reaches a steady state, another image (I_{dss}) is taken to provide a background C_o.

In order to disentangle the effects of the saturation and dye concentration levels on the emergent light intensity, the steady-state saturation must be determined in an image field on a pixel by pixel basis without dye (equation 2) and the concentration must be determined in the same manner, at the same steady-state (equation 4). In addition, adjustments must be made to the raw image to account for small changes in the light source over time. This adjustment is accomplished with the use of a standard light intensity wedge constructed of neutral density filters. This calibration wedge is present in all images and is illuminated by same light source that illuminates the sand slab.

PHYSICAL SYSTEM DESIGN AND EXPERIMENTAL SEQUENCE

Description of Experimental System

The experiment was conducted in a thin (0.953 cm) but extensive slab chamber (30x60 cm) fabricated out of 1/2 inch thick glass plate that was uniformly filled with a translucent silica sand through a randomizing extension [12]. The extension, attached to the top of the chamber, forces the sand to fall through a number of randomizing screens and pack evenly. The resultant sand pack characteristics were a bulk density of 1.61 g/ml and a porosity of 0.39. The sand passed through a 480μm sieve, was stopped by a 120μm sieve and had an approximate mean grain size of 250μm. The sides of the chamber were fitted with multiple ports to allow the free flow of air during unsaturated flow sequences. The bottom of the slab chamber was fitted with a porous plate. The top of the chamber was fitted with either a screen manifold for saturated permeability measurements or a porous plate for unsaturated downward infiltration experiments. Flow in and out of the chamber at both the top and bottom was controlled by computer operated solenoid valves.

A bank of high output fluorescent bulbs driven by high frequency (40,000 Hz) ballasts uniformly backlight the chamber. This light source was controlled by an electronic feedback loop to minimize light intensity changes with time. A solid state video camera captured the image at the front of the slab chamber in a 512 by 512 pixel format. Camera output was then digitized into gray level values between 0 and 255 by a dedicated processor board on a computer. The camera was positioned to resolve the chamber into 0.017 cm^2/pixel areas. Images can be acquired at time intervals as small as 1/30th of a second. Control of the solenoid valves, peristaltic pumps and scales used in the experiment was accomplished by the same computer used for image acquisition.

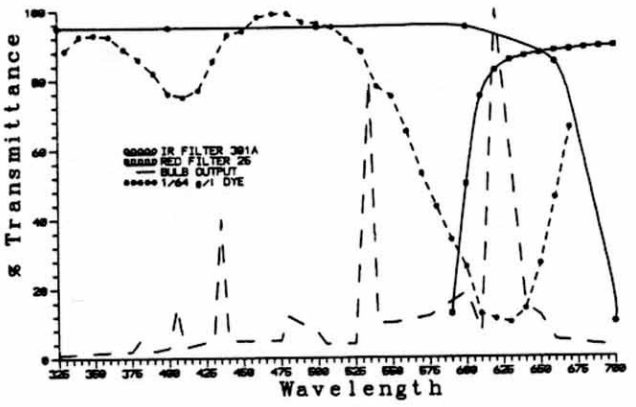

Figure 1. Light source output and percent transmittance of blue dye (1/64 g/l) and filters versus wavelength.

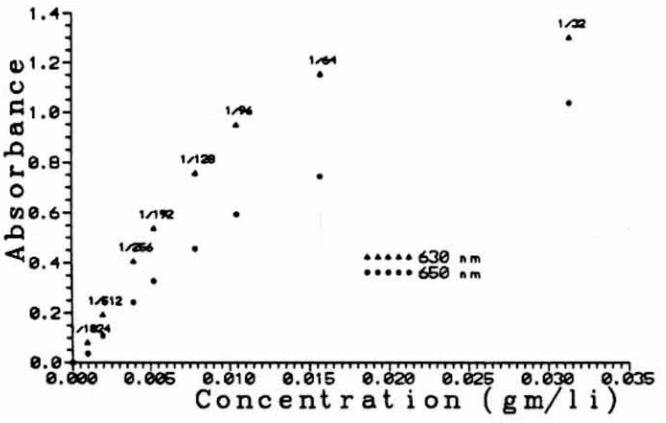

Figure 2. Beer's law, absorbance versus wavelength at 630 and 650 nm. for various concentrations of FD&C blue dye #1

Choice of Camera Filters and Dye

Figure 1 presents a plot of bulb output normalized to transmittance, the manufacture's transmittance data for the filter set used and spectrophotometric data on dye as a function of wavelength. The peak in bulb output seen at the 625 nm wavelength is immediately apparent. We sought to narrow the wavelengths seen by the camera system to approximate a monochromatic light source and make use of this high light level offered by the bulbs. The pass band we designed was made up of two separate filters, a 700 nm low pass and a 600 nm high pass filter.

The FD&C blue #1 dye chosen as the solute was found to exhibit minor, reversible chemical adsorption to the silica sand used in the experiments. An important characteristic of this dye was its high light absorption at low concentrations near the 625 nm wavelength. An area of maximum change in transmittance for a given change in dilute concentration was sought in order to avoid problems due to high dye concentrations. These problems include instabilities introduced due to density differences, potential problems with clearing the sand pack due to adsorption processes and physical limitations on the amount of incident light flux from behind the chamber. The spectrophotometric data in Figure 2 shows that the dye seen through the pass band does in fact follow a simple exponential Beer's law for dilute solutions (linear region) at two of the dominant wavelengths we are working at.

Experimental Sequence

The experimental sequence was begun from an air dry state with a series of two wetting and drying cycles. Digital images taken throughout this sequence were analyzed to determine the value of k for the moisture content calibration curve (equation 2) and to build pressure/saturation curves for the sand pack [15]. The chamber was then saturated with de-ionized water from the bottom and the upper screened manifold put in place. Flow into the bottom manifold was established, pressure differential across the pack measured, and the saturated hydraulic conductivity computed.

Once the saturated conductivity was measured, a sequence of flow and dye transport experiments were performed to build the relative permeability curve for the pack and evaluate the full-field dye concentration measurement technique. Because light attenuation is a function of both moisture content and dye concentration, the known moisture content field must be at a steady state in order to evaluate dye concentrations. Three one-dimensional, gravity-driven, steady-state unsaturated flow fields of different moisture content and one saturated flow field was established by adjusting the flow rate supplied to the chamber's top manifold. Each of these flow fields was established from the sand pack at its residual moisture content.

Once a steady-state flow field was established, the fluid was switched from DI water to dye and DI at a concentration of 1/32 g/l. Images of the transient dye concentration field for this line source were taken until the concentration in the chamber reached a constant value. The fluids were then switched back to clear and images of the flushing of the dyed water recorded. To minimize apparatus-induced dispersion and establish sharp concentration fronts during the introduction of dye, we implemented a two second "purge" of the top manifold when switching between fluids. Solenoid valves were first opened at the ends of the manifold and the fluids purged rapidly with minimal interruption of the flow into the chamber. The switch from clear DI fluid to dye and back again to clear constituted a two-sided step function that allows us to explore dispersion at both the front and back of the pulse.

RESULTS

Hydraulic Properties and Moisture Content Fields

From the initial fill and drain sequences, a k value for equation (2) of 18 was found to give a good match with volumetric measurements into and out of the chamber. Images taken during these sequences were also used to build the primary drainage and secondary wetting and drainage curves presented in figure 3. The chamber, when first filled, reached a saturation of 96%. The

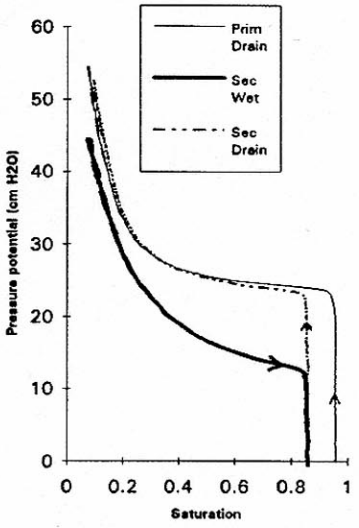

Figure 3. Moisture characteristic curve.

primary drainage curve was very steep, reaching a residual saturation of approximately 10%. The secondary wetting and drainage curves stayed below the primary drainage curve and displayed strong hysteresis. Filling the chamber from any moisture content greater than or equal to the residual moisture content decreases the final available saturation state to 87% due to entrapped air. Thus, once the chamber has been filled and drained the available states range between 10% and 87% saturation.

Saturation profiles for the steady-state gravity-driven flow fields established for the dye concentration experiments are given in figure 4. These plots were made by scanning the image horizontally at 0.12 cm. vertical increments. Average saturations for the entire chamber are shown on the figure. We refer to these averages to designate a particular steady-state flow field. A comparison between the 81% and 58% saturation profiles shows larger variations in amplitude in the 58% profiles suggesting a lower signal to noise ratio at lower saturations. All of the profiles range within about 10% of the average saturation, with the 81% case being the most uniform and the 75% case the most heterogeneous. In the 75% saturation experiment the bottom manifold did not supply an adequate suction nor have enough surface area to establish a single uniform moisture content throughout the chamber at the steady-state flow rate supplied. As a result the bottom third of the chamber neared saturation (≈81%) with the top at a lower moisture content(≈71%).

If we assume a uniform moisture content and a unit gradient, then the wetting-phase relative permeability of the pack is proportional to the flow rate. This assumption is reasonable given that the small moisture-content variations in the profiles correspond to

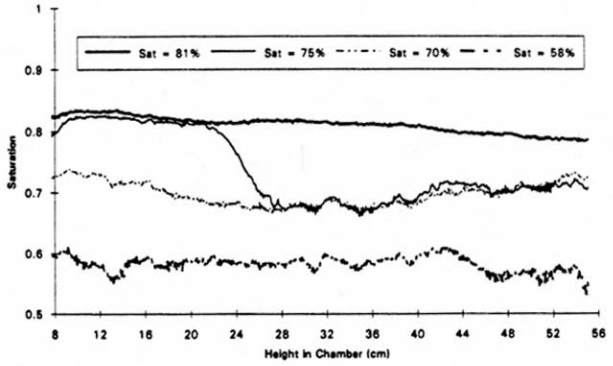

Figure 4. Vertical steady-state saturation profiles of chamber.

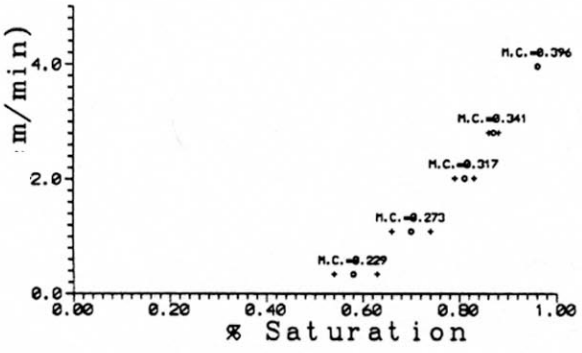

Figure 5. Wetting-phase relative permeability.

small differences in potential pressure, as seen on the secondary wetting curve of figure 3. Using this assumption, the relative permeability as a function of saturation was plotted along with the one standard deviation error associated with the saturation measurements made vertically within the chamber (Figure 5).

Concentration Fields and Profiles

Equation (4) was applied on a pixel by pixel basis to the light adjusted images throughout the sequences. Figure 6 presents a selection of C/C_0 image fields for both the front and back of the dye pulse from the 81% saturated experiment. Although details are difficult to see in black and white, the dispersion at the edge of the dye pulse clearly increases as the pulse moves through the chamber. A careful comparison of the front to the back end of the pulse images at later times shows that the back of the pulse is slightly more disperse than the front. Edge effects due to flow rate disturbance at the sides of the chamber are also more clearly defined in the images of the back of the pulse than in the images of the front.

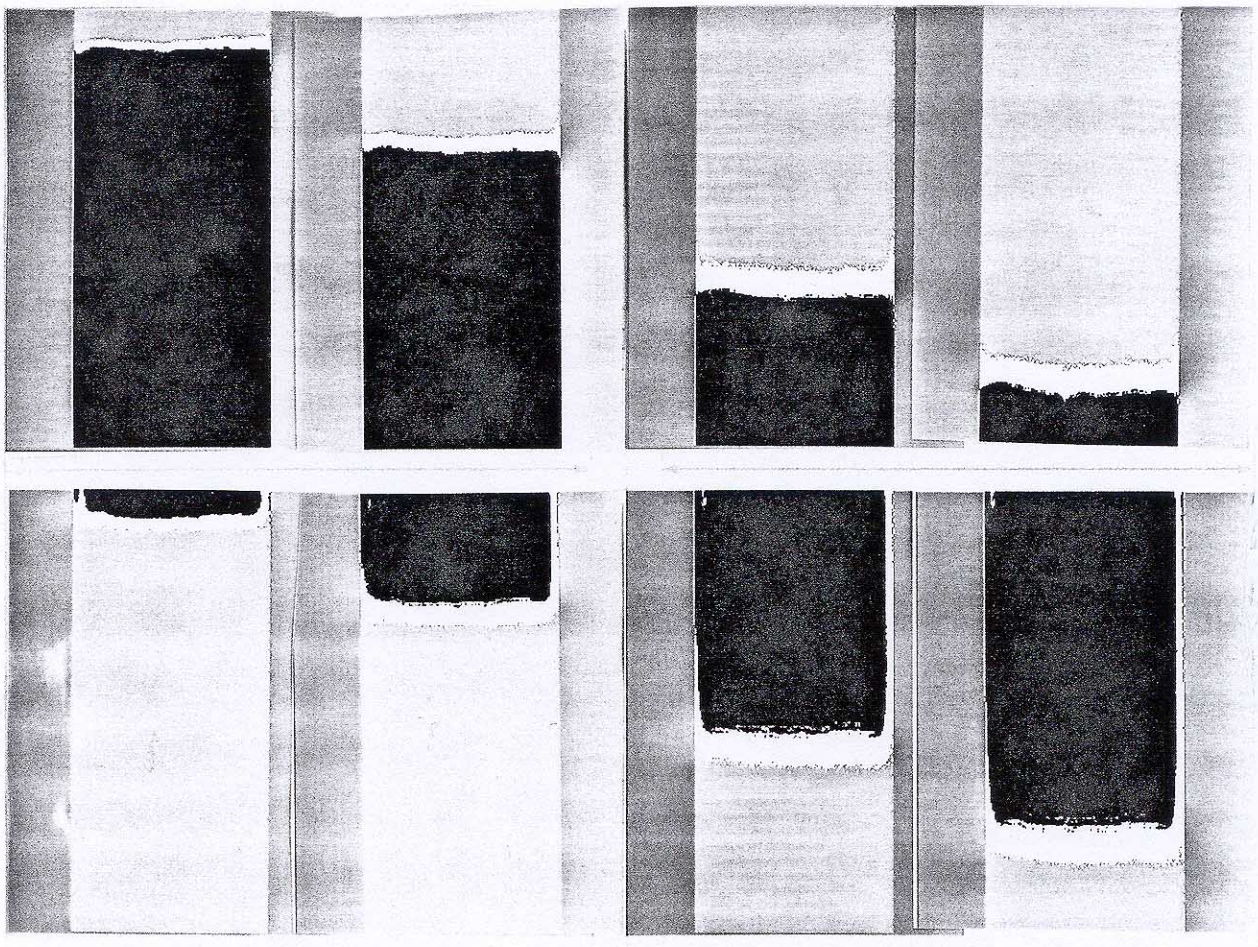

Figure 6. C/C_o images of the front of the dye plus at t=1, 3, 6 & 8 minutes; back of the pulse at t=1, 3, 6 & 8 minutes for the 81% saturation case.

Plotted in figure 7 are the C/C_o vertical profiles for the front and back of the pulse from the 81% saturated experiment. The C/C_o profiles clearly illustrate the development of the dispersive front as noted in the previous images. Translating an early and late C/C_o profile (at ≈10 and 55 cm) for each sequence to the same midpoint on the figure highlights the evolution of dispersion in the chamber (figure 8). The C/C_o profiles for the front and back of the pulse at the 81% saturation case are interesting. At first glance they seem roughly the same in shape and show approximately equal amounts of dispersion. Upon closer examination however, a stronger tailing of concentration at the back of the pulse can be seen. Comparing the front and back of pulse curves at t=1 reveals only slight tailing, at t=8 the effect is much more pronounced.

Figure 9 presents a time series of images as the dye pulse moves through the chamber for the 70% saturation experiment. Development of a non-uniform dispersive front is immediately apparent. At all moisture contents except 81%, the most saturated case, a similarly shaped waveform developed as the pulse moved through the chamber. The most saturated case used a top manifold with a screen, in all other cases a porous plate top manifold was used.

As a test of the accuracy of the technique we interrogated each image to determine the mass of dye as calculated by equation (4) and compared it to the known dye mass input. The mass of dye at each pixel within an image was determined by multiplying the concentration at that pixel by the volume of water it represented as determined from the saturation image. The mass of dye in each image was then summed and compared with the known dye mass based on gravimetric measurements. The percent difference between the calculated and known mass is presented in figure 10 and is discussed below.

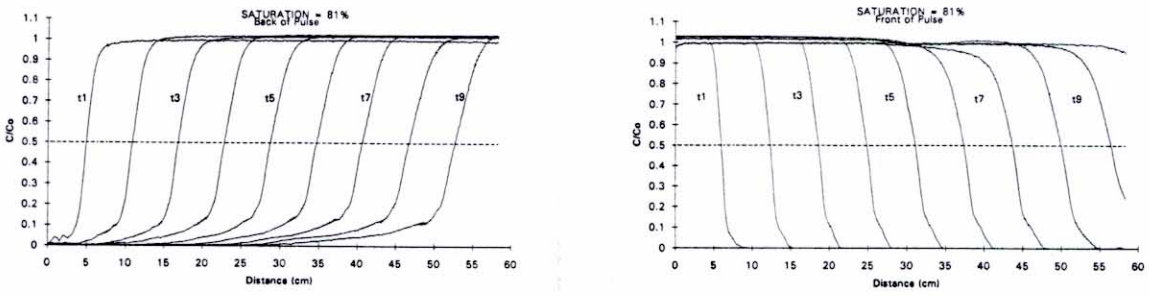

Figure 7. C/C_O verticle profiles for the front and back of the pulse at 81% saturation.

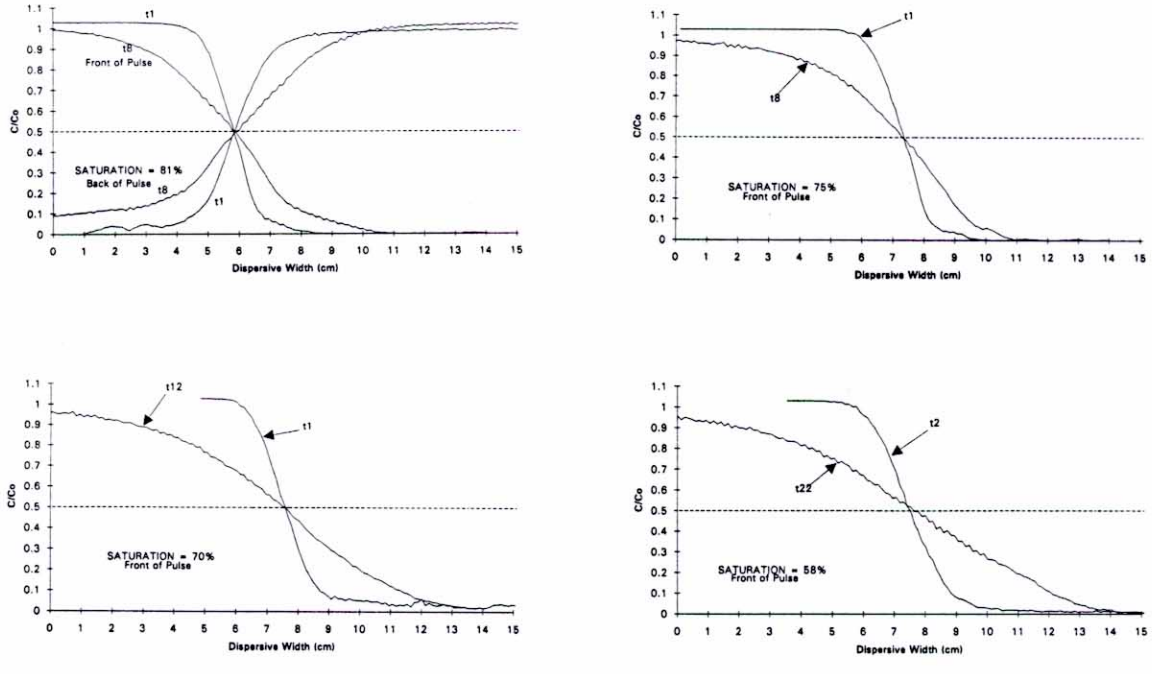

Figure 8. Translation for comparison of C/C_O profiles for an early and late profile (at ≈10 and 55 cm.) at 81%, 75%, 70% and 58% saturation.

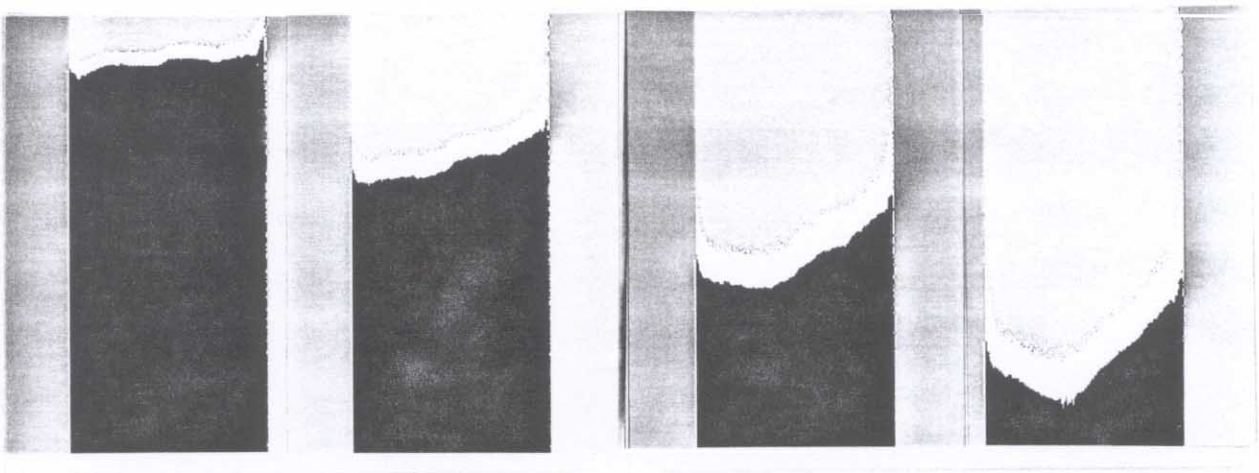

Figure 9. Waveform development at the front of the pulse for the 70% saturation experiment, t=2, 5, 8 and 11 minutes.

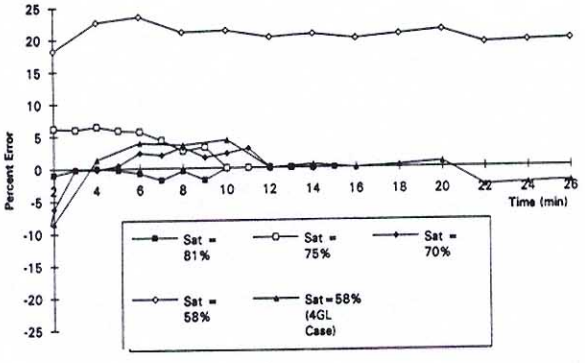

Figure 10. Percent error of dye mass, calculation based on image versus known input.

DISCUSSION OF CONCENTRATION FIELDS

Non-uniformity of dye pulse front

It was interesting to note the repeatability of the waveform dispersive front seen in Figure 9 at other degrees of saturation. As discussed earlier, an attempt was made to minimize the dispersion due to fluid mixing within the top porous plate manifold by flushing it momentarily (≈2 sec) when we switched fluids. In addition to this, great care was taken in making sure that the manifolds' porous plate made good contact with the porous media when the manifold was mounted. While not completely successful at controlling experimental artifacts we were at least consistent.

The shape of the front and its progressive growth suggests that a slight differential velocity field had developed in the chamber. The non-uniformity in flow seen here is probably present to some degree in all unsaturated experiments. A uniform fluid supply is very difficult to obtain experimentally. We expected to see some non-uniformity of flow at the edges of the porous plate but not in the middle. This type of variation in flow could occur if small bubbles were trapped in the manifold during flushing; if the hydraulic connection between the porous plate and the sand pack was disturbed; or if the permeability of the porous plate varied along its length.

Measurement of the dispersion due to the porous medium must not be confused with that caused by the boundary conditions. Non-uniform flow field effects on the C/C_o curves can be removed by selecting an appropriate region or window of the dispersive front to be examined. Two scanning windows were selected at approximately one-half and one-thirty second of the full image. The windows were then placed over a more linear area of the developing front. The difference caused by averaging across the entire chamber is significant. A one-half or one-thirty second of an image scan more accurately reflected the dispersive front for the 70% saturated experiment as the pulse neared the bottom of the chamber (figure 11).

Gravity Effects

The difference in density between the dye (1.0003 gm/ml) and clear (0.9996 gm/ml) DI fluids was measured and found to be very small. However, evidence that there may have been density effects in this experiment can be seen in the plot for the 81% saturated case presented in figure 7. All of the images profiled in these sequences were taken at one minute intervals. A careful

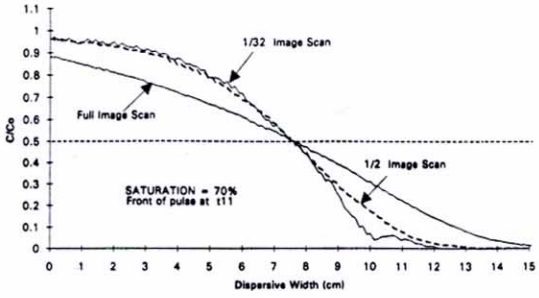

Figure 11. Translation for comparison of C/C_O profiles at t=11 for the windowed 70% saturation case.

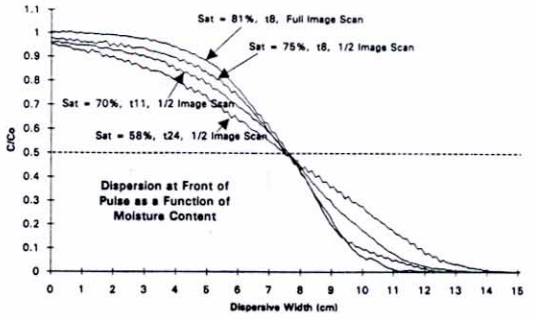

Figure 12. C/C_O profile as a function of moisture content appropriately windowed and scanned at ≈ 55 centimeters.

comparison of the plot for the dispersion taking place at the front of the pulse with that taking place at the rear seems to show that the dispersive front at the back of the pulse was moving through the chamber slower (5.1 cm/min. as scaled from the profile) than the front of the pulse (5.5 cm/min.). This gravity effect might also be involved in the differences seen between the tailing of the concentration profiles at front and back of the pulse.

Effects Due to Moisture Content

The effect of the abrupt change in moisture content for the 75% saturation case seen in figure 4 was evident in its time series profile plot. The increase in moisture content twenty five centimeters from the bottom of the chamber under steady-state flow conditions caused a decrease in velocity. This change was seen after about five minutes, the pulse front slowed down by 20% (percentage was scaled from the plot) as it moved through the region of higher moisture content. Velocities can be predicted from the simple expression $V=(Q/A)/\theta$ where the average flow rate was 41.0 ml/min., cross sectional area 25.7 cm^2 and theta take from saturation images to be approximately 0.279 (71% saturation) at the top of the chamber and 0.318 (81% saturation) at the bottom. Using these parameters yields velocities of 5.7 and 5.0 cm/min. respectively, a 13 percent change.

Figure 12 presents a comparison plot of the C/C_O profiles at all four of the moisture contents. These profiles were taken at approximately the same point in the chamber, about 55 centimeters from the top. A linear region of each of the developing fronts was windowed and scanned to extract the best possible profile. The increased dispersion due to a decrease in moisture content is clearly evident.

Mass Balance

Figure 10, presented earlier, shows the difference between calculated and known dye mass input into the chamber. There was agreement within about 5% at three of the four moisture contents. The large but constant error at the 58% saturation case may be due to using too high a dye concentration relative to the emergent light at this low moisture content. When we examine the steady-state images of clear water, we find the expected uniform drop in light intensity as a function of decreasing moisture content. However, this drop was not proportionally seen in the steady-state images of dyed water at the lowest saturation levels. Our hypotheses is that the optical system could not accurately resolve the dye in the chamber for the 58% saturation case because light levels fell below the sensitivity range of the camera. In order to test this theory we uniformly subtracted four gray-scale intensity levels, proportionate to the change seen in the clear field images, from the steady-state dye field and recomputed the dye mass throughout the sequence. The results, plotted in figure 10 as the 58%(4GL case), compared favorably to the uncorrected dye mass calculations at the other moisture contents.

CONCLUSIONS

We have developed an experimental technique based on light absorption of dye that provides exceptional spatial and temporal resolution of dye concentration in thin slabs of porous material. As can be seen in the images, the ability of the system to qualitatively capture and resolve the concentration fields is very good. Once captured, each image can be quantified to produce either saturation information or dye concentration information based on simple light absorption theory. The total mass of dye in the chamber was accurately predicted to within 5% using algorithms based on this theory. Selecting a vertical section of the image to window improved resolution in those cases when the front was non-horizontal due to a non-uniform flow field. Placing windows over the dispersive front allowed us to interrogate an image in enough detail to see increases in dispersion due to decreasing moisture content, tailing of dispersion at the rear of the dye pulse, and slight velocity changes of the dispersive front due to moisture content differences.

The dynamic range of available light intensity must be considered in choosing dye concentrations. An investigation into working with more dilute solutions where the response of the system is more linear should be made. However, the need for linearity in response has to balanced with the need for resolution between the dye field and the moisture content field. It is important to note that the physical chamber size for these experiments is not a major limiting factor. The optical system can easily be scaled up to any reasonable size in order to capture a more meaningful cross section of geologic material. A larger three-foot by three-foot system is now under construction. Although this paper deals with a homogeneous sand pack, homogeneity is not a required condition for the use of this technique. Manipulations on the images presented in this paper were done on a pixel by pixel basis. This can be just as easily accomplished for images of a very complex heterogeneous system. The only requirement to measure a dye field is that the moisture content field be at a steady state.

This laboratory technique allows systematic experimentation into the basic processes affecting solute transport within saturated/unsaturated porous media. Processing more complex steady-state moisture-content fields and dye pulses is being contemplated as the next logical step. This would involve resolving longitudinal and transverse dispersion associated with a half-field source or point injection of dye into a one or two dimensional steady-state moisture-content field and accurately accounting for the dye mass. The future challenge for this work will be to use these techniques to analyze more complex systems involving heterogeneities, scaling laws and detailed investigations of the relationship between transverse and longitudinal dispersion in unsaturated media.

ACKNOWLEDGMENTS

The research was performed under appointment to the Civilian Radioactive Waste Management Fellowship program sponsored by the Office of Civilian Radioactive Waste Management of the U.S. Department of Energy administered by Oak Ridge Institute for Science and Education.

The authors would like to acknowledge the help of University of New Mexico students Jim Brainard and David Lopez for their help in the development and proving of the experimental sub-systems, Jon Woodroof and John O'Rourke for their work with image data over and above the call of duty and Lee Orear of Sandia National Laboratory for his patience in programming the experimental systems and image processing algorithms.

REFERENCES

1. L. W. GELHAR AND C. L. AXNESS, "Three-dimensional stochastic analysis of macrodispersion in aquifers", WRR, February, 1983

2. G. DAGAN, "Theory of solute transport by groundwater", Ann. Rev. Fluid. Mech., 1987

3. G. SPOSITO AND D. A. BARRY, "On the Dagan model of solute transport in groundwater: Foundational aspects", WRR, October, 1987

4. A. A. BAKR, L. W. GELHAR, A. L GUTJAHR AND J. MACMILLAN, "Stochastic analysis of spatial variability in subsurface flows 1. Comparison of one and three-dimensional flows", WRR, April, 1978

5. O. GUVEN AND F. MOLTZ, "Deterministic and stochastic analysis of dispersion in an unbounded stratified porous medium", WRR, October, 1986

6. S. P. NEUMAN, L. C WINTER AND C. NEWMAN, "Stochastic theory of field-scale fickian dispersion in anisotropic porous media", WRR, March, 1987

7. G. DAGEN, "Transport in heterogeneous porous formations: spatial moments, ergodicty and effective dispersion", WRR, June, 1990

8. G. DAGAN, "Stochastic modeling of groundwater flow by unconditional and conditional probabilities, 2) The solute transport", WRR, August, 1982

9. T.-C. YEH, L. W. GELHAR AND A. L. GUTJAHR, "Stochastic analysis of unsaturated flow in heterogeneous soils", WRR, Part 1,2 and 3, April, 1985

10. J. W. HOPMANS, H. SCHUKKING, AND P. J. J. F. TORFS, "Two-dimensional steady state unsaturated water flow in heterogeneous soils with autocorrelated soil hydraulic properties", WRR, December, 1988

11. L. W. GELHAR, "Stochastic subsurface hydrology from theory to application", WRR, August, 1986

12. E. A. SUDICKY, AND P. S. HUYAKORN, "Contaminant migration in imperfectly known heterogenious groundwater systems", Reviews of Geophysics, April, 1991, pp240-253

13. R. J GLASS, "Laboratory research program to aid in developing and testing the validity of conceptual models for flow and transport through unsaturated porous media", Proc. of GEOVAL-90 Symposium, Stockholm, Sweden, 1990, pp275-284

14. R. J. GLASS, T. S STEENHUIS, AND J-Y PARLANGE, "Mechanism for finger persistence in homogeneous unsaturated porous media: Theory and Verification", Soil Science, V148, 1989

15. V. C. TIDWELL AND R. J. GLASS, "X-ray and visible light transmission as two-dimensional, full-field moisture-sensing techniques: A preliminary comparison", Proc. of the Third Int. High Level Radioactive Waste Mgmt. Conference, April, 1992, Las Vegas, Nevada